

1 **Recharge estimation and soil moisture dynamics in a**
2 **Mediterranean karst aquifer**

3 Fabian Ries^{1,2}, Jens Lange¹, Sebastian Schmidt², Heike Puhmann³ and Martin Sauter²

4 [1] {Chair of Hydrology, University of Freiburg, Freiburg, Germany}

5 [2] {Geoscience Center, Applied Geology, University of Göttingen, Göttingen, Germany}

6 [3] {Forest Research Institute Baden-Württemberg, Freiburg, Germany}

7 Correspondence to: F. Ries (fabian.ries@hydrology.uni-freiburg.de)

8

9 **Abstract**

10 Knowledge of soil moisture dynamics in the unsaturated soil zone provides valuable
11 information on the temporal and spatial variability of groundwater recharge. This is especially
12 true for the Mediterranean region, where a substantial fraction of long-term groundwater
13 recharge is expected to occur during high magnitude precipitation events of above-average
14 wet winters. To elucidate process understanding of infiltration processes during these extreme
15 events, a monitoring network of precipitation gauges, meteorological stations, and soil
16 moisture plots was installed in an area with a steep climatic gradient in the Jordan Valley
17 region. In three soil moisture plots, Hydrus-1D was used to simulate water movement in the
18 unsaturated soil zone with soil hydraulic parameters estimated by the Shuffled Complex
19 Evolution Metropolis algorithm. To generalize our results, we modified soil depth and rainfall
20 input to simulate the effect of the pronounced climatic gradient and soil depth variability on
21 percolation fluxes and applied the calibrated model to a time series with 62 years of
22 meteorological data.

23 Soil moisture measurements showed a pronounced seasonality and suggested rapid infiltration
24 during heavy rainstorms. Hydrus-1D successfully simulated short and long-term soil moisture
25 patterns, with the majority of simulated deep percolation occurring during a few intensive
26 rainfall events. Temperature drops in a nearby groundwater well were observed
27 synchronously with simulated percolation pulses, indicating rapid groundwater recharge
28 mechanisms. The 62-year model run yielded annual percolation fluxes of up to 66 % of
29 precipitation depths during wet years and of 0 % during dry years. Furthermore, a dependence
30 of recharge on the temporal rainfall distribution could be shown. Strong correlations between
31 depth of recharge and soil depth were also observed.

1 Introduction

In the Mediterranean region, groundwater is the main source for domestic and agricultural water supplies (EUWI, 2007). Knowledge on the quantity of groundwater recharge is a prerequisite for sustainable water resources planning and effective water use. Small-scale differences in climate, geology, land use, topography and soil properties cause a high spatial and temporal variability of groundwater recharge making the assessment and predictions of recharge a challenge (e.g. Zagana et al., 2007). Karst areas are important in this respect, because during high intensity winter storms precipitation may rapidly infiltrate into exposed karst surfaces and induce high recharge rates (De Vries and Simmers, 2002), which are common in the Mediterranean area (Ford and Williams, 2007). A rapidly increasing water demand in the last decades has led to a widespread overexploitation of groundwater resources (EUWI, 2007). Furthermore, the Mediterranean region has been identified as a “hot spot” of current and future climate change (Giorgi, 2006; IPCC, 2013), imposing additional pressure on its limited water resources. Hence, more insights into processes of aquifer replenishment in Mediterranean karst regions are of vital importance.

A large variety of methods suitable for estimating recharge rates were developed in the last decades (De Vries and Simmers, 2002; Scanlon et al., 2002). Infiltration, percolation and recharge quantities in Mediterranean karst have mainly been approached from two sides: On the one hand, hydrologists and geomorphologists characterized the surface water balance on small plots by sprinkling experiments or by runoff/sediment measurements during natural rainstorms (e.g. Cerdà, 1998; Lavee et al., 1998). Large-scale experiments also included tracers and facilitated statements on runoff generation processes (e.g. Lange et al., 2003). However, these studies quantified infiltration by the difference between artificial/natural rainfall and measured overland flow but did not differentiate between recharge and evapotranspiration. On the other hand, hydrogeologists frequently assessed average recharge rates of entire karst catchments from spring discharge measurements or hydraulic head data. Methods include knowledge (GIS)-based mapping (Andreo et al., 2008), multiple linear regression (Alloca et al., 2014), conceptual models (e.g. Hartmann et al., 2013a), coupled water-balance groundwater models (Sheffer et al., 2010), and chloride mass balances (Marei et al., 2010; Schmidt et al., 2013). However, these studies treat karst systems as units, including both the unsaturated and the saturated zones, and are limited in temporal and spatial resolution. Studies on cave drips (Gregory et al., 2009; Arbel et al., 2010; Lange et al., 2010) provided insights into the deeper unsaturated zone in terms of water storage, spatial variability of percolation and flow paths. Their data was also used to incorporate variability in recharge modelling (Hartmann et al., 2012). However, it was difficult to distinguish between processes in the unsaturated soil zone and in the underlying epikarst, and uncertainty remains regarding the representativeness of cave drip data with respect to infiltration processes. This is mainly due to the facts that the contributing areas of cave drips are unknown and caves might have

Formatted: Highlight

1 developed their own hydraulic environments. Therefore cave drips are not necessarily
2 representative for the bulk karst vadose zone (Lange et al., 2010).

3 Only limited knowledge on recharge dynamics is available for the carbonate aquifer system
4 shared between the West Bank and Israel. First recharge estimates were based on long-term
5 spring discharge and groundwater well abstraction data (Goldschmidt and Jacobs, 1958).
6 Later, groundwater flow models were used to establish empirical rainfall-recharge
7 relationships (Baida and Burstein, 1970; Guttman and Zukerman, 1995; Zukerman, 1999).
8 Average recharge rates were assessed by a simple water balance approach (Hughes et al.,
9 2008) and by a chloride mass balance (Marei et al., 2010). Seheffer et al. (2010) coupled a
10 water budget model with a groundwater flow model for the entire Western part of the
11 carbonate aquifer and used spring discharge and groundwater level data for calibration. They
12 reported recharge rates ranging between 9 % and 40 % of annual rainfall and showed that the
13 temporal distribution of rainfall within the winter season had considerable effects on overall
14 recharge rates.

15 Observations of soil moisture may offer unique insights into near surface hydrological
16 processes, because water fluxes are susceptible to conditions and properties of the vadose soil
17 zone across several scales (Vereecken et al., 2008). Yet, soil moisture is rarely measured in
18 semi-arid areas and is seldom used for recharge estimation purposes. Scott et al. (2000)
19 exemplified the potential of soil moisture time series to calibrate Hydrus-1D soil hydraulic
20 parameters in southeastern Arizona. Youval Arbel monitored soil moisture during his study
21 for temporal changes in infiltration. Their results demonstrated the high inter-annual
22 variability of water fluxes in these environments where considerable percolation only occurs
23 during above-average wet years.

Formatted: Highlight

24 The objective of this study is to investigate the spatial and temporal variability of percolation,
25 and hence groundwater recharge rates, for an Eastern Mediterranean carbonate aquifer. We
26 use continuously recorded soil moisture data to calibrate one-dimensional water flow models
27 (Hydrus-1D) with the Shuffled Complex Evolution Metropolis (SCEM) algorithm. The
28 calibrated models are then used to assess spatial and temporal patterns of soil water
29 percolation in a Mediterranean karst area, which is characterized by strong climatic gradients
30 and variable soil depths.

31 2 Study area

32 Our study area is located on the western margin of the Jordan Rift Valley 25 km northeast of
33 Jerusalem (Figure 1). Precipitation shows a pronounced seasonality with cold fronts (mainly
34 Cyprus lows) carrying moisture from the Mediterranean Sea during winter season from
35 October to April (Goldreich, 2003). The topographic gradient from the mountain range
36 (highest elevation: 1016 m a.s.l.) in the west to the Jordan Valley in the east results in a strong
37 precipitation gradient generating a rain-shadow desert. Long-term average annual

Formatted: Highlight

1 precipitation decreases from 532 mm in Jerusalem (810 m a.s.l.) to 156 mm in Jericho (290 m
2 b.s.l.) (Morin et al., 2009).

3 Rainfall intensities??

4 The area is also affected by the Red Sea Trough system from the south during autumn and
5 spring

Formatted: Highlight

6 Evaporation??

Formatted: Highlight

7 Outcropping geological formations consist of carbonate rocks of the Upper Cretaceous age
8 (Begin, 1975). They are composed of fractured and highly permeable layers of limestone and
9 dolomite alternating with marl and chalk layers of low permeability, often considered partial
10 aquicludes (Weiss and Gvirtzman, 2007). ~~In the southeast, Senonian C~~chalks ~~form outcrops~~
11 of low hydraulic conductivity outcrop in the southeast (Rofe and Raffety, 1963). Soil parent
12 material consists of residual clay minerals from carbonate rock weathering and from the
13 aeolian input of dust (silt and clay fraction) chemical composition of dust??? originating from
14 the Sahara desert (Yaalon, 1997). Predominant soil types are Terra Rossa and Rendzina, both
15 characterized by high ??? ranges?? clay contents. Terra Rossa more clay Rendzina less
16 Rendzina soils contain carbonate in the soil matrix ranges??, are thinner and still show recent
17 development, whereas Terra Rossa soils were formed under past climatic conditions (Yaalon,
18 !!!!!!! Shapiro, 2006). As a result of the diverse, irregular underlying carbonate rock, degree
19 of weathering and heterogeneous topography, soil depth is highly variable. The slopes are
20 covered by ~~On the slopes, outcropping~~ massive bedrock exposures, and loose rock fragments
21 of different sizes alternating ~~e~~ with soil pockets of variable dimensions, shapes, and depths
22 ranges??? (Figure 2). Dissolution cracks and karst fissures are often filled with eroded soil
23 material – actually the soil pockets develop above dissolution cracks. In valley bottoms, fine
24 textured alluvial soils (Vertisols) with soil depths up to several meters have developed.
25 Shallow Brown Lithosols and loessial Arid Brown Soils dominate in the eastern, low-lying
26 areas receiving less rainfall (Shapiro, 2006). In general, soils in the region have significantly
27 been affected transformed by human activities such as land cultivation, terracing, and
28 deforestation during the last 5000 years (Yaalon, 1997).

Formatted: Highlight

Formatted: Highlight

Formatted: Highlight

Formatted: Highlight

Formatted: Highlight

Formatted: Highlight

Formatted: Highlight

29 On the hillslopes, annual plants and Mediterranean shrubs (predominantly *Sarcopoterium*
30 *spinosum*) are the dominant vegetation types. They are used for extensive grazing by goats
31 and sheep. South-facing slopes show ~~a~~ lower vegetation density and ~~a~~ higher proportion of
32 bare soil and rock outcrops than the north-facing slopes, where the presence of biogenic crusts
33 was reported (Kutiel et al., 1998). Minor land use types consist of scattered built-up areas,
34 olive plantations on terraced land and rainfed or partly irrigated agricultural land (annual and
35 perennial crops, herbs and vegetables) in valley bottoms.

36 **3 Material and methods**

3.1 Hydrometeorological measurements

To capture the spatial variation of rainfall along the strong climatic gradient, we installed a rain gauge network consisting of 14 tipping buckets (RG3-M) connected to a HOBO pendant event data logger (Onset Computer Corporation) (Figure 1). All gauges were calibrated before employment, maintained, and cleaned twice a year before and after the rainfall season. Temperature was measured at four climatic stations (Thies GmbH and Onset Computer Corporation). Additional rainfall and climatic data was obtained from the Israel Meteorological Service database (<http://www.data.gov.il/ims>) for long-term analyses. Additionally, groundwater levels and temperatures were recorded in a nearby well (Mini-Diver, Eijkelkamp).

3.2 Soil moisture measurements

Seven soil moisture plots were installed, each equipped with four capacitance soil moisture sensors (5TM/5TE, Decagon Devices Inc.). We paid attention that the plots did not receive lateral surplus water from upslope overland flow by placing them distant from rock outcrops and at locations with minimum slopegradient. To minimize disturbance, we inserted the sensors vertically into the upslope wall of manually dug soil pits (depth between 35 and 80 cm). After installation, we refilled the pits with the parent soil material and compacted approximately to pre-disturbance bulk density. The probes were connected to data loggers (EM50, Decagon Devices Inc.), which were sealed by plastic bags and buried in the soil to avoid vandalism. We used the internal calibration function for mineral soils with a measurement accuracy of 4 % of the volumetric water content (VWC). The measurement interval was set at ten minutes. Further information on the performance of the employed sensors can be found in Kizito et al. (2008). Due to instrument malfunction and vandalism, we obtained continuous data of our entire measurement period (October 2011 to May 2013) from only three locations (SM1–SM3). Characteristics of the plots are summarized in Table 1.

The dielectric permittivity of water changes with temperature (e.g. Wraith and Or, 1999). Hence, measurement techniques of soil moisture based on the difference of dielectric permittivity between water and soil matrix are affected by this phenomenon. In our case, soil temperature was highly variable and changed by up to 20 °C within 24 hours due to a strong radiation input and partly uncovered soil. We corrected our soil moisture data applying multiple linear regressions against soil temperature as described by Cobos and Campell (2007).

3.3 Modelling of the soil zone

Water balance at the plot scale in absence of surface runoff can be described with:

$$\frac{ds}{dt} = P - E_a - L \quad \text{with} \quad E_a = E_i + E_s + E_t, \quad (1)$$

1 where ds/dt is the storage change over time, P is the precipitation, L is the percolation at the
2 profile bottom and E_a is the evapotranspiration per time interval. E_a is composed of the terms
3 E_i (evaporation of intercepted precipitation), E_s (soil evaporation) and E_t (plant transpiration).

4 For our three soil moisture plots, soil water content and water fluxes were simulated on a
5 daily basis with Hydrus-1D (version 4.16; Šimůnek et al., 2013) for a period of 32 months.
6 Hydrus-1D solves the Richards equation numerically for water transport in variable saturated
7 media. Matric potential dependent water retention and hydraulic conductivity were calculated
8 using the Mualem/van-Genuchten soil hydraulic model (van Genuchten, 1980). To reduce the
9 effect of non-linearity of the hydraulic conductivity function close to saturated conditions, an
10 air entry value of -2 cm as suggested by Vogel et al. (2001) was used. Interception by the
11 plant canopy was calculated by an empirical equation including the leaf area index and daily
12 precipitation values (see Šimůnek et al., 2013 for more details). Potential evapotranspiration
13 was calculated by the Hargreaves-equation (Hargreaves and Samani, 1985). Originally
14 developed for a lysimeter station in California, this method adequately reproduced potential
15 evapotranspiration under semi-arid climates (Jensen et al., 1997; Weiß and Menzel, 2008).
16 Potential evapotranspiration was split into potential evaporation from the soil surface and
17 potential transpiration from plants according to Beer's law based on the time variable surface
18 cover fraction. Both fluxes were reduced to actual values based on a root water uptake model
19 (Feddes et al., 1978) applying plant parameters for grass and an energy balance surface
20 evaporation model (Camillo and Gurney, 1986). In our study area, vegetation cover shows a
21 strong seasonality due to the restricted water availability during the dry season. To account
22 for this, time dependent plant growth data was implemented into the model with intra-annual
23 variation of surface cover fraction. According to field observations, the start of the growing
24 season was set to mid November and the maximum vegetation density was assumed for
25 February/March shortly after the largest monthly precipitation amounts were observed. The
26 depth from which plants took up water was controlled by a root distribution function. An
27 exponential decrease of root density with soil depth was assumed, observed at the study sites
28 and often reported for the Mediterranean region (e.g. De Rosnay and Polcher, 1998; De Baets
29 et al., 2008). Temporal variations of rooting depth and root density were disregarded. With
30 these components, Hydrus-1D continuously computed water content and water fluxes at user
31 defined observation points (here: depths of the soil moisture probes) and at the lower profile
32 boundary. Model input data, selected parameter values and their ranges, and the
33 corresponding data sources and calculation methods are summarized in Table 2.

34 **3.4 Calibration procedure, uncertainty analysis and parameter sensitivity**

35 An increase of clay content and bulk density with depth was observed at all profiles and the
36 individual probes in various depths at our plots differed noticeably. As a result, a particular
37 soil material with singular soil hydraulic properties was assigned for each soil moisture probe.
38 Documented Observed soil moisture data from two winters and one summer season (October

1 2011 to April 2013) were used for calibration of Hydrus-1D. We individually determined soil
 2 hydraulic parameters for every soil material by inverse modelling using the Shuffled Complex
 3 Evolution Metropolis optimization algorithm (SCEM; Vrugt et al., 2003) and the Kling-Gupta
 4 efficiency (KGE; Gupta et al., 2009) in a modified version from Kling et al. (2012) as the
 5 objective function:

$$6 \quad KGE = 1 - \frac{r - 1^2 + \alpha - 1^2 + \beta - 1^2}{r - 1^2 + \alpha - 1^2 + \beta - 1^2} \quad (2)$$

7 with:

$$8 \quad r = \frac{Cov_{so}}{\sigma_s \sigma_o}, \alpha = \frac{\mu_s}{\mu_o} \text{ and } \beta = \frac{\sigma_s / \mu_s}{\sigma_o / \mu_o},$$

9 where r is the correlation coefficient between simulated and observed VWC (Cov_{so} is the
 10 covariance between simulated and observed VWC), α is a dimensionless measure for the bias
 11 (μ_s and μ_o are the mean simulated and observed VWC) and β is a dimensionless measure for
 12 variability (σ_s and σ_o are the standard deviations of simulated and observed VWC). SCEM is
 13 widely used to efficiently solve global optimization problems (e.g. Vrugt et al., 2005;
 14 Schoups et al., 2005; Feyen, 2007; Hartmann et al., 2012) and to find optimal model
 15 parameter sets. As algorithmic parameters for SCEM, 24 complexes/parallel sequences were
 16 selected (equal to the number of parameters to be optimized), the population size was set to
 17 144 and the number of accepted draws to infer posterior distribution was set to 1000. The
 18 SCEM routine was run until the scale reduction score (SR), a convergence criterion defined
 19 by Gelman and Rubin (1992), was fulfilled. As proposed by Vrugt et al. (2003), a SR value of
 20 1.2 was chosen, indicating that the Markov chain had converged to a stationary posterior
 21 distribution for all parameters. Predicted soil moisture ranges were used for parameter
 22 uncertainty assessment. They were determined by running Hydrus-1D with 1000 parameter
 23 sets obtained through the SCEM algorithm after reaching convergence.

24 3.5 Spatial and temporal extrapolation of percolation

25 To extrapolate our point measurements of soil water balance, we varied soil depth and
 26 climatic input parameters (precipitation and temperature) over ranges observed in our study
 27 area. We used the calibrated soil hydraulic parameters of our deepest (1 m) soil moisture plot
 28 (SM-1), which had sensors at 10, 25, 40 and 80 cm. Moreover, we assumed that the rooting
 29 depth was limited to the soil depth with no changes in the vertical root distribution or plant
 30 surface cover fraction. We cut off the profile according to the simulated soil depth, which
 31 reduced the number of independent soil layers when the depths fell below 60, 32.5 and
 32 17.5 cm. For soil thicknesses exceeding 1 m, we extended the bottom layer. To simulate the
 33 range of climatic conditions with elevations between 400 and 1000 m a.s.l., we modified
 34 rainfall and air temperature according to calculated mean annual gradients based on observed
 35 rainfall and climatic data. We had three seasons of measured climate data, which we analysed
 36 separately due to seasonal differences in cumulative rainfall amount and distribution.

1 Using a 62-year record of rainfall and temperature (1951–2013) available for Jerusalem
2 (Israel Meteorological Service – www.data.gov.il/ims), we assessed the annual variability of
3 water balance components at the location of our three soil moisture plots. Rainfall and
4 temperature data from Jerusalem station were corrected for elevation differences between the
5 Jerusalem station (810 m a.s.l.) and the three plots based on calculated elevation gradients.

1 4 Results

2 4.1 Hydrometeorological conditions

3 The three years of high resolution measurements of precipitation and meteorological
4 parameters revealed considerable interannual variability and a strong elevation gradient,
5 especially in terms of rainfall the further we go eastward away from the Mediterranean. Mean
6 annual precipitation at the Kafr Malek station (810 m a.s.l.) situated close to the
7 Mediterranean Sea–Dead Sea water divide was 526 mm (380–650 mm), while mean annual
8 rainfall at the Auja Village station (270 m b.s.l.) in the Jordan Valley accounted for 106 mm
9 (97–120 mm) leading to seasonal rainfall gradients between 6.4 % to 7.2 % per 100 m
10 elevation difference (Figure 3). Mean annual temperature was 7 °C higher at Auja Village
11 whereas relative humidity, wind speed, and net solar radiation were slightly higher at the
12 more elevated station. Stations from the Israel Meteorological Service with long-term records
13 at nearby locations nearby where???? showed similar characteristics.

Formatted: Highlight

14 4.2 Soil moisture dynamics

15 Observed soil moisture at all soil profiles (Figure 4) showed a strong seasonality where the
16 annual course can be divided into distinct phases. At the beginning of the rainy season, the
17 previously dry soil profile was stepwise wetting up starting from the upper to the lower
18 sensors. During rainfall events with high amounts and intensities, the soil moisture data
19 showed rapid infiltration of water into the deeper portions of the profile. Particularly at plot
20 SM-1, saturated conditions started from the bottom probe close to the soil-bedrock interface,
21 where these conditions persisted for several hours up to two days. During the strongest
22 rainfall events also upper soil layers reached saturation, however for much shorter periods
23 (Figure 4b). At the end of the rainy season, the soil dried was drying out within a few weeks
24 and the soil moisture content further declined at a low rate during the whole dry summer
25 period.

26 4.3 Modelling of the soil zone

27 4.3.1 Parameter optimization, uncertainty analysis and model validation

28 Soil hydraulic parameters were optimized for the three soil moisture plots individually, using
29 the Shuffled Complex Evolution Metropolis algorithm. Between 20,000 and 36,000 model
30 runs were conducted until the convergence criterion was fulfilled. The calibrated parameter
31 sets used for further assessment of the plot scale soil water balance, are given in Table 3, and
32 their distributions are illustrated in Figure 5. All models were generally able to reproduce the
33 observed temporal soil moisture patterns with KGE values between 0.82 and 0.94 (Figure 6).
34 However, differences in predictive capacities at distinct water content levels could be
35 observed, which vary between the single plots (Figure 6 and Figure 7). In general, the model

1 tended to overestimate water contents close to saturated conditions except for deeper sections
2 at plot SM-1 where an underestimation of simulated water contents was observed.

3 Parameter uncertainty was assessed by simulation of water contents using parameter sets
4 obtained with SCEM after fulfilling the convergence criterion. The 95 % soil moisture
5 confidence interval showed a narrow band around the optimum model (Figure 8 exemplary
6 for plot SM-1). At all sensors the difference between simulated volumetric water content for
7 the best parameter set and the 95 % confidence interval remained below 4 %, i.e. less than the
8 measurement error of the sensors.

9 Water temperature in a groundwater well near soil moisture plot SM-3 (cf. Figure 1) indicated
10 five distinct recharge events lowering the mean groundwater temperature from 19 °C by 0.7–4
11 °C (Figure 7). These events coincided with the main peaks of modelled percolation from the
12 soil moisture monitoring sites. During these events, mean daily air temperature was less than
13 6 °C.

14 **4.3.2 Plot scale water balance**

15 Modelled fluxes of the various water balance components showed high temporal variability
16 (Figure 8) and considerable differences in annual values between single years (Table 4).
17 Evaporation and transpiration started shortly after the first rainfall events of the winter season
18 when the water content in the upper soil layer began to increase. Percolation from the bottom
19 of the soil zone only started after the cumulative rainfall during winter season exceeded a
20 certain threshold. This threshold was found to be ca. 240 mm at plot SM-1, 200 mm at plot
21 SM-2, and 150 mm at plot SM-3. The relative proportion of interception, soil evaporation,
22 and transpiration was highly variable during the winter season, depending on the length of dry
23 spells between rainfall events and ceased within few weeks after the last rainfall events of the
24 winter season. Mean overall losses through evapotranspiration and interception accounted for
25 73 % of rainfall. Values slightly above 100 % for the dry year 2010/2011 resulted from
26 elevated moisture conditions at the beginning of the simulation period. Percolation strongly
27 varied from negligible amounts during the dry year 2010/2011 (how dry – annual rainfall
28 relative to average) to values ranging between 28 % and 45 % of cumulative rainfall during
29 2011/2012 and 2012/2013, respectively. The largest proportion of percolation was calculated
30 during a few strong rainstorms. On all three plots, more than 50 % of the total percolation of
31 the three years simulation period occurred within a time period of five to ten days.

32 **4.3.3 Spatial extrapolation of deep percolation**

33 During the hydrological year 2010/2011, cumulative rainfall was below average with totals
34 ranging between 275 and 425 mm (Figure 9) and a maximum daily amount below 50 mm. In
35 this season with below average rainfall amounts, percolation was only simulated for soils with
36 depths up to 60 and 110 cm, respectively. Modelled percolation increased to a maximum

1 proportion of 40 % for shallow soils with depths of 10 cm receiving the highest rainfall input.
2 For the following above-average wet year 2011/2012, seasonal rainfall ranged between 450
3 and 725 mm. Then simulated percolation rates reached up to 69 % of rainfall and declined to
4 values close to 0 % only under conditions of lowest rainfall amount and soil depths greater
5 than 160 cm. The third simulated year can be regarded as a year with average rainfall
6 conditions (sums of 400 to 600 mm). Percentages of percolation were comparable to the
7 previous year although cumulative rainfall was considerably less. This could be attributed to
8 higher rainfall intensities during 2012/2013 when daily rainfall amounts exceeded ~~twice~~
9 ~~times~~ 80 mm a day –and four days of rainfall accounted for almost 50 % of the seasonal
10 amount.

11 **4.3.4 Temporal extrapolation of deep percolation**

12 Modelling water balance components for 62 years (1951-2013) resulted in strong differences
13 of simulated seasonal percolation reflecting the high variability of rainfall input (Figure 10).
14 Mean annual rainfall was calculated for the three plots to range between 408 and 537 mm
15 (standard deviation: 128–168 mm) and mean percolation fluxes between 82 and 150 mm
16 (standard deviation: 93–141 mm). Percolation at the three plots varied between 0 % and 66 %
17 of cumulative seasonal rainfall with an average between 16 % and 24 %. Other seasonal
18 fluxes varied much less during the simulation period. The coefficient of determination
19 between seasonal sums of simulated percolation and rainfall ranged between 0.82 and 0.88 on
20 the three plots.

21 **5 Discussion**

22 **5.1 Soil moisture dynamics**

23 The observed seasonal dynamics of soil moisture, dominated by short wetting phases during
24 and a rapid decrease after the rainfall season, were comparable with those reported in other
25 studies in the Mediterranean region (Cantón et al., 2010; Ruiz-Sinoga et al., 2011). At all soil
26 moisture plots, our soil moisture data suggested fast infiltration into deeper sections of the soil
27 profile during rainfall events with high intensities and amounts (e.g. plot SM-1 in Figure 4b).
28 The time lag between the reaction of the uppermost and the lowermost probe was often less
29 than two hours despite high clay contents of the soils. These fast reactions might be an
30 indicator for concentrated infiltration and preferential flow within the vadose soil zone as
31 reported for the Mediterranean by Cerdá et al. (1998), Öhrström et al. (2002) and Van Schaik
32 et al. (2008). Nevertheless, larger macropores were rarely observed in the field and superficial
33 desiccation cracks that appeared during dry summer months closed soon after the beginning
34 of the rainfall season. Moreover, a successive propagation of the wetting front was observed
35 at the plots that gave no indication of significant bypass flow as reported by e.g. Booltink and
36 Bouma (1991) for structured clay soils. Brilliant Blue patterns from infiltration experiments

1 | conducted in the vicinity of our plots supported these findings (Sohrt et al., 2014). These
2 | experiments highlighted the influence of outcrops on infiltration by initiating preferential flow
3 | at the soil-bedrock interface, while the remaining soil matrix was largely unaffected. Hence, a
4 | high stone content in the soil and bedrock outcrops in the vicinity, as observed particularly at
5 | SM-1, may have multiple effects on infiltration, water retention and water movement in the
6 | soil (Cousin et al., 2003).

7 | A noticeable difference between the plots was observed during rainfall events of high
8 | magnitude. At SM-1 (Figure 4b), the bottom probe suggested soil saturation for periods
9 | between 2 and 90 hours. Durations were apparently linked to the depth of the event
10 | precipitation (24 to 191 mm) and to the duration of the event (16 to 72 h). The upper probes
11 | showed saturation only during the largest rainfall events and for a much shorter duration.
12 | Volumetric soil moisture at 10 cm always remained below 30%. We observed a similar
13 | behaviour at SM-3 but not at SM-2. We hypothesize that these phases of saturation were
14 | caused by impounded percolation water due to limited conductivity of the soil-bedrock
15 | interface. Differences between our plots could be attributed to differences in the permeability
16 | of the underlying ~~strata. These are~~ Cenomanian dolomite (SM-1 and SM-3) and Turonian
17 | limestone (SM-2). While both formations are known to have high permeability (Keshet and
18 | Mimran, 1993), we observed Nari Crust (Dan, 1977) in the vicinity of SM-1, which may have
19 | reduced hydraulic conductivity. Sprinkling experiments on the same geological material type
20 | had already documented soil saturation and subsequent overland flow generation (Lange et
21 | al., 2003).

22 | **5.2 Simulation of the plot scale water balance**

23 | The cumulative distribution functions of the parameters suggested rather narrow ranges and
24 | hence good identifiability for most model parameters (Figure 5). Nevertheless, measured soil
25 | moisture fell outside the 95% uncertainty band especially during high and low moisture
26 | conditions (Figure 8). This suggests that a Mualem/van-Genuchten soil hydraulic model based
27 | on a unimodal pore-size distribution may not be able to represent the heterogeneous pore
28 | structure of our clay-rich soil (Durner, 1994). Moreover, persistent saturated conditions
29 | during major rainstorms as discussed in the previous section could not be simulated, as a
30 | percolation impounding soil-rock interface was not implemented in the model and a free
31 | drainage had to be assumed.

32 | Simulated mean evapotranspiration at our plots over the three_-years simulation period
33 | accounted for 73 % of rainfall, i.e. very close to the long-term average calculated by Schmidt
34 | et al. (2014) for the same area. Our values also fall into the range of Cantón et al. (2010), who
35 | derived annual effective evapotranspiration rates of more than 64 % of annual rainfall based
36 | on eddy covariance measurements in southeastern semi-arid Spain. Our simulated percolation
37 | rates ranged between 0 % and 45 % of precipitation (arithmetic mean: 28 %) indicating strong

1 inter-annual variability and a strong dependency on depth and temporal distribution of
2 precipitation. During the entire three year period, more than 50 % of overall percolation
3 fluxes occurred during less than 10 days of strong rainfall. These findings are supported by
4 the response of groundwater temperatures observed in a nearby well indicating the arrival of
5 groundwater recharge flux at the water table (Figure 8). Tracer experiments in a similar
6 setting demonstrated that percolating water can pass the vadose soil and the epikarst at flow
7 velocities of up to 4.3 m/h (Lange et al., 2010). Regarding the initiation of percolation at the
8 basis of the soil profiles, we found seasonal rainfall thresholds of ca. 150 mm for the shallow
9 and 240 mm for the deep soil moisture plots. Cave drip studies in the region (Arbel et al.,
10 2010; Lange et al., 2010; Sheffer et al., 2011) measured similar thresholds for the initiation of
11 percolation through the epikarst (100 to 220 mm).

12 In contrast to humid environments, lateral subsurface flow on rocky semi-arid hillslopes
13 rarely develops, since they consist of individual soil pockets that are poorly connected due to
14 frequently bedrock outcrops. ping bedrocks. Soil moisture seldom exceeds field capacity
15 given that evapotranspiration exceeds precipitation depth throughout most of the year
16 (Puigdefabregas et al., 1998). Furthermore, highly permeable bedrocks favour the
17 development of vertical structural pathways in karst areas (dolines, sinkholes) inducing
18 concentrated infiltration from the soil zone (Williams, 1983). We can therefore conclude that
19 one-dimensional modelling of the soil water balance is a reasonable approach to understand
20 percolation and recharge.

21 Nevertheless, we cannot exclude that frequently outcropping bedrock may affect water
22 redistribution by surface runoff or by preferential infiltration along the soil-rock interface. The
23 importance of these effects on percolation rates and groundwater recharge on the regional
24 scale is subject to current research. During heavy storm events, overland flow generation
25 cannot be excluded (Lange et al., 2003), but surface runoff typically accounts for only a few
26 percent of annual rainfall (Gunkel and Lange, 2012). A second limitation of our investigations
27 of plot scale percolation fluxes is the assumption of an identical vegetation cover at the single
28 sites along the climatic gradient and a constant vegetation cycle throughout years of different
29 seasonal rainfall depths. Although different plant species and vegetation cycles may alter soil
30 moisture conditions prior to rainfall events, we could show that the event rainfall amount is
31 the main factor that influences percolation rates.

32 **5.3 Spatial and temporal extrapolation of deep percolation**

33 Water balance modelling for variable soil depths and rainfall gradients revealed considerable
34 differences for the three winter seasons. During the very dry year 2010/2011, soil moisture
35 exceeded field capacity only at locations with relatively shallow soils. During the wet years of
36 2011/2012 and 2012/2013, field capacity was exceeded several times at all plots and soils
37 even reached saturation during strong rainfall events. This may lead to substantial percolation

1 and groundwater recharge to local aquifers. These findings are in good agreement with
2 discharge measurements at Auja spring, a large karst spring in the Jordan Valley, **on the**
3 **map???** where 7 and 8 million m³ yr⁻¹ were measured for the winter seasons 2011/2012 and
4 2012/2013 respectively, but only 0.5 million m³ yr⁻¹ for the 2010/2011 season (Schmidt et al.,
5 2014).

Formatted: Highlight

Formatted: Superscript

Formatted: Superscript

6 A high temporal variability in percolation fluxes is also apparent from the long-term
7 modelling of water balance components (Figure 11). For the 62-year simulation period, we
8 calculated seasonal percolation rates between 0 % and 66 % (average: 20 % to 28 %) for our
9 plots. The highest value was modelled for the extremely wet winter season 1991/1992 (five
10 times the mean annual percolation of 150 mm). For a slightly shorter time period, Schmidt et
11 al. (2014) calculated an average recharge rate of 33 % for the Auja spring catchment **using**
12 **with** a conceptual reservoir model. They found that recharge of only five individual years
13 accounted for one third of **the** total recharge of the 45-years period. In our study seven
14 individual years provided one third of the total recharge. Furthermore, we compared seasonal
15 percolation of our sites with recharge estimations from perched aquifers feeding small karst
16 springs (Weiss and Gvirtzman, 2007) and the entire carbonate aquifer (Guttman und
17 Zukerman, 1995) (Figure 11). Although our results plotted within the range of these large-
18 scale recharge estimates, we want to emphasize that our calculations display point percolation
19 fluxes. Even in years with below-average rainfall, a certain rise in the groundwater table and
20 spring flow can be observed (EXACT, 1998; Schmidt et al. 2014). Then recharge presumably
21 occurs on areas with strongly developed epikarst and shallow or missing soil cover.

22 Our long-term point calculations suggest substantial differences in percolation fluxes between
23 years of similar rainfall depths. Simulated percolation for plot SM-1 during the seasons
24 1976/1977 and 2004/2005 accounted for 16 % and 35 % of seasonal rainfall, respectively,
25 although both seasons had very similar above-average rainfall (578 and 569 mm). These
26 results are in line with findings of Sheffer et al. (2010) and Abusaada (2011) about the
27 importance of temporal rainfall distribution on groundwater recharge.

28 5.4 Implications for recharge in Mediterranean karst areas

29 The steep climatic gradient, the hydraulic properties and characteristics of the carbonate
30 rocks, the heterogeneous soil cover and **at the** high temporal variability of precipitation on
31 event and seasonal scales are dominating hydrological characteristics in our study area.
32 Similar settings can be found across the entire Mediterranean region. Despite recent advances
33 in the determination of groundwater recharge in karst areas, the assessment of the spatial and
34 temporal distribution of recharge is still a challenge. Modelling approaches including
35 hydrochemical and isotopic data (Hartmann et al., 2013b) require additional information from
36 springs (time series of discharge and water chemistry) for model parameter estimation, which
37 are rarely available. Although simulated percolation fluxes from plot-scale soil moisture

1 | measurements cannot be directly transferred to regional, i.e. catchment scale, they can still
2 | provide an insight into the various processes responsible for the temporal and spatial
3 | variability of groundwater recharge as well as information on the relative importance of
4 | different process parameters.

6 Conclusions

This study contributes to the assessment of percolation rates based on soil moisture measurements along a steep climatic gradient in a Mediterranean karst area. We showed that soil moisture measurements together with numerical modelling of the water flow in the unsaturated soil zone are powerful tools to investigate mechanisms and characteristics determining the strong annual variability in the percolation fluxes and the strong dependency on soil thickness, temporal distribution of rainfall and precipitation depth. Although our calculations are based on plot scale measurements, the results closely match long-term observations and the patterns of event and seasonal variability, and reflect the thresholds for the initiation of groundwater recharge reported by other studies in the same region based on different approaches. Our results suggest that groundwater recharge is most prominent when single rainfall events are strong enough to exceed field capacity of soil pockets over a wide range of soil depths. Furthermore, our data revealed that the temporal distribution of rainfall had a strong effect on event and seasonal recharge amounts.

We therefore corroborate the statement of De Vries and Simmers (2002) about the dependence of groundwater recharge in semi-(arid) areas on high intensity rainfall events.

Thresholds of intensities? If the intensities are too high which can happen in this region especially in autumn and spring we get runoff and then a reduction in infiltration The use of empirical rainfall-recharge relationships can lead to large errors, since recharge rates are sensitive with respect to highly variable rainfall distributions and characteristics, which are most probably affected by predicted climate change in the Mediterranean (Giorgi and Lionello, 2008; Samuels et al., 2011; Reiser and Kutiel, 2012). **How about using high rainfall-depth events rather than high-intensity events?**

Formatted: Highlight

Formatted: Highlight

Formatted: Highlight

Acknowledgements

This work is conducted within the context of the multi-lateral research project “SMART – Sustainable Management of Available Water Resources with Innovative Technologies” funded by BMBF (German Federal Ministry of Education and Research), references No. 02WM0802 and 02WM1081. The first author was partially supported by the BMFB–MOST Young Scientist Exchange Program during a two-month stay at the University of Haifa/Israel. The article processing charge was funded by the German Research Foundation (DFG) and the Albert Ludwigs University Freiburg in the funding programme Open Access Publishing. Furthermore we want to thank Amer Fraejat, Awad Rashid, Kayan Manasra and Clemens Messerschmid for hospitality and support during fieldwork.

1 References

- Abusaada, M. J.: Flow Dynamics and Management Options in Stressed Carbonate Aquifer System, The Western Aquifer Basin, Palestine. PhD Thesis, University of Göttingen, 2011.
- Allen, R. G., Pereira, L. S., Raes, D. and Smith, M.: Crop Evapotranspiration: Guidelines for Computing Crop Water Requirements, Irrigation and Drainage Paper 56, FAO, Rome, 1998.
- Allocca, V., Manna, F. and De Vita, P.: Estimating annual groundwater recharge coefficient for karst aquifers of the southern Apennines (Italy), *Hydrol. Earth Syst. Sci.*, 18, 803–817, 2014.
- Andreo, B., Vías, J., Durán, J. J., Jiménez, P., López-Geta, J. A. and Carrasco, F.: Methodology for groundwater recharge assessment in carbonate aquifers: application to pilot sites in southern Spain, *Hydrogeol. J.*, 16, 911–925, 2008.
- ANTEA: Well Development Study of the Eastern Aquifer Basin, Northern Districts of Palestine, vol. 1, Interim Report, Conceptual Model, unpublished ANTEA Report No. A11903, 1998.
- Arbel, Y., Greenbaum, N., Lange, J. and Inbar, M.: Infiltration processes and flow rates in developed karst vadose zone using tracers in cave drips, *Earth Surf. Process. Landf.*, 35, 1682–1693, 2010.
- Baida, U. and Burstein, Y.: The Yarkon Taninim aquifer in Be'er Sheva, calibrating and flow model, unpublished report in Hebrew, TAHAL Consulting Engineers Ltd. 01/95/72, Tel Aviv, Israel, 1970.
- Begin, Z. B.: The geology of the Jericho sheet, Geological Survey of Israel, Bulletin No. 67, Jerusalem, 1975.
- Booltink, H. W. G. and Bouma, J.: Physical and morphological characterization of bypass flow in a well-structured clay soil, *Soil Sci. Soc. Am. J.*, 55, 1249–1254, 1991.
- Camillo, P. J. and Gurney, R. J.: A resistance parameter for bare-soil evaporation models, *Soil Sci.*, 141, 742–744, 1986.
- Cantón, Y., Villagarcía, L., Moro, M. J., Serrano-Ortíz, P., Were, A., Alcalá, F. J., Kowalski, A. S., Solé-Benet, A., Lázaro, R. and Domingo, F.: Temporal dynamics of soil water balance components in a karst range in southeastern Spain: estimation of potential recharge, *Hydrol. Sci. J.* 55, 737–753, 2010.

- Cerdà, A., Schnabel, S., Ceballos, A. and Gomez-Amelia, D.: Soil hydrological response under simulated rainfall in the Dehesa land system (Extremadura, SW Spain) under drought conditions, *Earth Surf. Process. Landf.*, 23, 195–209, 1998.
- Cerdà, A.: Effect of climate on surface flow along a climatological gradient in Israel: a field rainfall simulation approach, *J. Arid Environ.*, 38, 145–159, 1998.
- Cobos D. R. and Campbell C.: Correcting temperature sensitivity of ECH2O soil moisture sensors, Application Note #800-755-2751, Decagon Devices, Pullman, WA, 2007.
- Cousin, I., Nicoullaud, B. and Coutadeur, C.: Influence of rock fragments on the water retention and water percolation in a calcareous soil, *Catena*, 53, 97–114, 2003.
- Dan, J.: The distribution and origin of Nari and other lime crusts in Israel, *Isr. J. Earth Sci.*, 26, 68–83, 1977.
- De Baets, S., Poesen, J., Reubens, B., Wemans, K., De Baerdemaeker, J. and Muys, B.: Root tensile strength and root distribution of typical Mediterranean plant species and their contribution to soil shear strength, *Plant Soil*, 305, 207–226, 2008.
- De Rosnay, P. and Polcher, J.: Modelling root water uptake in a complex land surface scheme coupled to a GCM, *Hydrol. Earth Syst. Sci.*, 2, 239–255, 1998.
- De Vries, J. J. and Simmers, I.: Groundwater recharge: an overview of processes and challenges, *Hydrogeol. J.*, 10, 5–17, 2002.
- Durner, W.: Hydraulic conductivity estimation for soils with heterogeneous pore structure, *Water Resour. Res.*, 30, 211–223, 1994.
- EUWI – European Water Initiative: Mediterranean groundwater report, technical report on groundwater management in the Mediterranean and the Water Framework Directive. Produced by the Mediterranean Groundwater Working Group, 2007. www.semide.net/initiatives/medeuwi/JP/GroundWater (Accessed 9 April 2014)
- EXACT – Executive Action Team: Overview of Middle East Water Resources – Water Resources of Palestinian, Jordanian, and Israeli Interest, compiled by the US Geological Survey for the Executive Action Team, Washington, p. 44. ISBN: 0-607-91785-7, 1998.
- Feddes, R.A., Kowalik, P.J. and Zaradny, H.: Simulation of field water use and crop yield, PUDOC, Wageningen, Simulation Monographs, pp. 189, 1978.
- Feyen, L., Vrugt, J. A., Nualláin, B. Ó., van der Knijff, J. and De Roo, A.: Parameter optimisation and uncertainty assessment for large-scale streamflow simulation with the LISFLOOD model, *J. Hydrol.*, 332, 276–289, 2007.

- Ford, D. C. and Williams, P. W.: *Karst Hydrogeology and Geomorphology*, Wiley, Chichester, 2007.
- Gelman, A. and Rubin, D. B.: Inference from iterative simulation using multiple sequences, *Stat. Sci.*, 7, 457–472, 1992.
- Giorgi, F. and Lionello, P.: Climate change projections for the Mediterranean region, *Glob. Planet. Chang.*, 63, 90–104, 2008.
- Giorgi, F.: Climate change hot-spots, *Geophys. Res. Lett.*, 33, L08707, doi:10.1029/2006GL025734, 2006.
- Goldreich, Y.: *The Climate of Israel: Observation research and application*, Kluwer Academic Press, London, pp. 270, 2003.
- Goldschmidt, M.J. and Jacobs, M.: Precipitation over and replenishment of the Yarqon and Nahal Hatteninim underground catchments, *Hydrological Paper 3*, Hydrological Service of Israel, Jerusalem, 1958.
- Gregory, L., Wilcox, B. P., Shade, B., Munster, C., Owens, K. and Veni, G.: Large-scale rainfall simulation over shallow caves on karst shrublands, *Ecohydrology*, 2, 72–80, 2009.
- Gunkel, A. and Lange, J.: New insights into the natural variability of water resources in the Lower Jordan River Basin, *Water Resour. Manage.*, 26, 963–980, 2012.
- Gupta, H. V., Kling, H., Yilmaz, K. K., and Martinez, G. F.: Decomposition of the mean squared error and NSE performance criteria: Implications for improving hydrological modelling, *J. Hydrol.*, 377, 80–91, 2009.
- Guttman, Y. and Zukerman, C. H.: Flow model in the Eastern Basin of the Judea and Samaria hills, unpublished report in Hebrew, TAHAL Consulting Engineers Ltd. 01/95/66, Tel Aviv, Israel, 1995.
- Hargreaves, G. H. and Samani, Z. A.: Reference crop evapotranspiration from temperature, *Appl. Eng. Agr.* 1, 96–99, 1985.
- Hartmann, A., Lange, J., Weiler, M., Arbel, Y. and Greenbaum, N.: A new approach to model the spatial and temporal variability of recharge to karst aquifers, *Hydrol. Earth Syst. Sci.*, 16, 2219–2231, 2012.
- Hartmann, A., Wagener, T., Rimmer, A., Lange, J., Brielmann, H. and Weiler, M.: Testing the realism of model structures to identify karst system processes using water quality and quantity signatures, *Water Resour. Res.* 49, 3345–3358, 2013a.

- Hartmann, A., Weiler, M., Wagener, T., Lange, J., Kralik, M., Humer, F., Mized, N., Rimmer, A., Barberá, J. A., Andreo, B., Butscher, C. and Huguenberger, P.: Process-based karst modelling to relate hydrodynamic and hydrochemical characteristics to system properties, *Hydrol. Earth Syst. Sci.*, 17, 3305–3321, 2013b.
- Hughes, A. G., Mansour, M. M. and Robins, N. S.: Evaluation of distributed recharge in an upland semi-arid karst system: the West Bank Mountain Aquifer, Middle East, *Hydrogeol. J.*, 16(5), 845–854, 2008.
- IPCC. Climate Change 2013: The Physical Science Basis. Contribution of Working Group I to the Fifth Assessment Report of the Intergovernmental Panel on Climate Change, edited by: Stocker, T. F., D. Qin, G.-K. Plattner, M. Tignor, S. K. Allen, J. Boschung, A. Nauels, Y. Xia, V. Bex and P. M. Midgley, Cambridge University Press, Cambridge, 1535 pp., 2013.
- IMS – Israel Meteorological Service: Online database of the Israel Meteorological Service, Bet Dagan, <http://data.gov.il/ims/3> (Accessed 1 March 2014)
- Jensen, D. T., Hargreaves, G. H., Temesgen, B. and Allen, R. G.: Computation of ETo under nonideal conditions, *J. Irrig. Drain. Eng.*, 123, 394–400, 1997.
- Keshet, N. and Mimran, Y.: Landuse mapping – Ramallah area, unpublished report in Hebrew, Geological Survey of Israel, GSI/14/93, Jerusalem, 1993.
- Kizito, F., Campbell, C. S., Campbell, G. S., Cobos, D. R., Teare, B. L., Carter, B. and Hopmans, J. W.: Frequency, electrical conductivity and temperature analysis of a low-cost capacitance soil moisture sensor, *J. Hydrol.*, 352, 367–378, 2008.
- Kling, H., Fuchs, M. and Paulin, M.: Runoff conditions in the upper Danube basin under an ensemble of climate change scenarios, *J. Hydrol.*, 424, 264–277, 2012.
- Kutiel, P., Lavee, H. and Ackermann, O.: Spatial distribution of soil surface coverage on north and south facing hillslopes along a Mediterranean to extreme arid climatic gradient, *Geomorphology*, 23, 245–256, 1998.
- Lange, J., Arbel, Y., Grodek, T. and Greenbaum, N.: Water percolation process studies in a Mediterranean karst area, *Hydrol. Process.*, 24, 1866–1879, 2010.
- Lange, J., Greenbaum, N., Husary, S., Ghanem, M., Leibundgut, C. and Schick, A. P.: Runoff generation from successive simulated rainfalls on a rocky, semi-arid, Mediterranean hillslope, *Hydrol. Process.*, 17, 279–296, 2003.
- Lavee, H., Imeson, A. C. and Sarah, P.: The impact of climate change on geomorphology and desertification along a Mediterranean-arid transect, *Land Degrad. Develop.*, 9, 407–422, 1998.

- Marei, A., Khayat, S., Weise, S., Ghannam, S., Sbaih, M. and Geyer, S.: Estimating groundwater recharge using the chloride mass-balance method in the West Bank, Palestine, *Hydrol. Sci. J.*, 55, 780–791, 2010.
- Morin, E., Jacoby, Y., Navon, S. and Bet-Halachmi, E.: Towards flash-flood prediction in the dry Dead Sea region utilizing radar rainfall information, *Adv. in Water Resour.*, 32, 1066–1076, 2009.
- Öhrström, P., Persson, M., Albergel, J., Zante, P., Nasri, S., Berndtsson, R. and Olsson, J.: Field-scale variation of preferential flow as indicated from dye coverage, *J. Hydrol.*, 257, 164–173, 2002.
- Puigdefabregas, J., del Barrio, G., Boer, M. M., Gutiérrez, L., Solé, A.: Differential responses of hillslope and channel elements to rainfall events in a semi-arid area, *Geomorphology* 23, 337–351, 1998.
- Reiser, H., and Kutiel, H.: The dependence of annual total on the number of rain spells and their yield in the Mediterranean, *Geografiska Annaler: Series A, Phys. Geogr.*, 94, 285–299, 2012.
- Rofe and Raffety Consulting Engineers: Jerusalem and District Water Supply: Geological and Hydrological Report. Report to the Central Water Authority of the Hashemite Kingdom of Jordan, London, 1963.
- Ruiz-Sinoga, J. D., Martínez-Murillo, J. F., Gabarrón-Galeote, M. A. and García-Marín, R.: The effects of soil moisture variability on the vegetation pattern in Mediterranean abandoned fields (Southern Spain), *Catena*, 85, 1–11, 2011.
- Samuels, R., Smiatek, G., Krichak, S., Kunstmann, H. and Alpert, P.: Extreme value indicators in highly resolved climate change simulations for the Jordan River area, *J. Geophys. Res. Atmos.*, 116, <http://dx.doi.org/10.1175/2010JHM1177.1>, 2011.
- Scanlon, B. R., Healy, R. W. and Cook, P. G.: Choosing appropriate techniques for quantifying groundwater recharge, *Hydrogeol. J.*, 10, 18–39, 2002.
- Schmidt, S., Geyer, T., Marei, A., Guttman, J. and Sauter, M.: Quantification of longterm wastewater impacts on karst groundwater resources in a semi-arid environment by chloride mass balance methods, *J. Hydrol.* 502, 177–190, 2013.
- Schmidt, S., Geyer, T., Guttman, J., Marei, A., Ries, F. and Sauter, M.: Characterisation and modelling of conduit restricted karst aquifers – example of the Auja spring, Jordan Valley, *J. Hydrol.*, 511, 750–763, 2014.

- Schoups, G., Hopmans, J. W., Young, C. A., Vrugt, J. A. and Wallender, W. W.: Multi-criteria optimization of a regional spatially-distributed subsurface water flow model, *J. Hydrol.*, 311, 20–48, 2005.
- Scott, R. L., Shuttleworth, W. J., Keefer, T. O. and Warrick, A. W.: Modeling multiyear observations of soil moisture recharge in the semiarid American Southwest, *Water Resour. Res.*, 36, 2233–2247, 2000.
- Shapiro, M. B.: Soils of Israel, *Eurasian Soil Sci.*, 39, 1170–1175, 2006.
- Sheffer, N. A., Cohen, M., Morin, E., Grodek, T., Gimburg, A., Magal, E., Gvirtzman, H., Nied, M., Isele, D. and Frumkin, A.: Integrated cave drip monitoring for epikarst recharge estimation in a dry Mediterranean area, Sif Cave, Israel, *Hydrol. Process.*, 25, 2837–2845, 2011.
- Sheffer, N. A., Dafny, E., Gvirtzman, H., Navon, S., Frumkin, A. and Morin, E.: Hydrometeorological daily recharge assessment model (DREAM) for the Western Mountain Aquifer, Israel: Model application and effects of temporal patterns, *Water Resour. Res.*, 46, W05510, doi:10.1029/2008WR007607, 2010.
- Šimůnek, J., Šejna, M., Saito, H., Sakai, M. and van Genuchten, M. Th.: The Hydrus-1D software package for simulating the movement of water, heat, and multiple solutes in variably saturated media, version 4.16, HYDRUS Software Series 3, Department of Environmental Sciences, University of California Riverside, Riverside, California, USA, pp. 340, 2013.
- Sohrt, J., Ries, F., Sauter, M. and Lange, J.: Significance of preferential flow at the rock soil interface in a semi-arid karst environment, submitted to *Catena*, 2014.
- van Genuchten, M. Th.: A closed-form equation for predicting the hydraulic conductivity of unsaturated soils, *Soil Sci. Soc. Am. J.*, 44, 892–898, 1980.
- Van Schaik, N. L. M. B., Schnabel, S. and Jetten, V. G.: The influence of preferential flow on hillslope hydrology in a semi-arid watershed (in the Spanish Dehesas), *Hydrol. Process.*, 22, 3844–3855, 2008.
- Vereecken, H., Huisman, J. A., Bogaen, H., Vanderborght, J., Vrugt, J. A. and Hopmans, J. W.: On the value of soil moisture measurements in vadose zone hydrology: A review, *Water Resour. Res.*, 44, W00D06, doi:10.1029/2008WR006829, 2008.
- Vogel, T., van Genuchten, M. T. and Cislerova, M.: Effect of the shape of the soil hydraulic functions near saturation on variably-saturated flow predictions, *Adv. Water Resour.*, 24, 133–144, 2001.

- Vrugt, J. A., Diks, C. G., Gupta, H. V., Bouten, W. and Verstraten, J. M.: Improved treatment of uncertainty in hydrologic modeling: Combining the strengths of global optimization and data assimilation, *Water Resour. Res.*, 41, 2005.
- Vrugt, J. A., Gupta, H. V., Bouten, W. and Sorooshian, S.: A Shuffled Complex Evolution Metropolis algorithm for optimization and uncertainty assessment of hydrologic model parameters, *Water Resour. Res.*, 39, 2003.
- Weiss, M. and Gvirtzman, H.: Estimating ground water recharge using flow models of perched karstic aquifers, *Ground Water*, 45, 761–773, 2007.
- Wei, M. and Menzel, L.: A global comparison of four potential evapotranspiration equations and their relevance to stream flow modeling in semi-arid environments, *Adv. Geosci.* 18, 15–23, 2008.
- Williams, P. W.: The role of the subcutaneous zone in karst hydrology, *J. Hydrol.*, 61, 45–67, 1983.
- Wraith, J. M. and Or, D.: Temperature effects on soil bulk dielectric permittivity measured by time domain reflectometry: A physical model, *Water Resour. Res.*, 35, 371-383, 1999.
- Yaalon, D. H.: Soils in the Mediterranean region: what makes them different? *Catena*, 28, 157–169, 1997.
- Zagana, E., Kuells, Ch., Udluft, P., Constantinou, C.: Methods of groundwater recharge estimation in eastern Mediterranean - a water balance model application in Greece, Cyprus and Jordan, *Hydrol. Process.*, 21, 2405–2414, 2007.
- Zukerman, C. H.: Yarqon-Tanninim-Beer Sheva Basin, Flow Model Update, unpublished report in Hebrew, TAHAL Consulting Engineers Ltd. 6759/700/133, Tel Aviv, Israel, 1999.

1 **Tables**

2 **Table 1.** Soil moisture plot characteristics.

Plot	Elevation (m a.s.l.)	Average annual rainfall^a (mm)	Soil depth (cm)	Sensor depths (cm)	Vegetation	Description
SM-1	810	526	100	10, 25, 40, 80	Mediterranean shrubs; annual plants	Sand: 20% Silt: 40% Clay: 40%
SM-2	660	340 ^b	50	5, 10, 20, 35	Annual plants	Sand: 32% Silt: 33% Clay: 35%
SM-3	440	351	60	5, 10, 20, 35	Annual plants	Sand: 46% Silt: 24% Clay: 30%

3 ^a Mean rainfall based on three winter seasons (2010-2013).

4 ^b Rainfall at plot SM-2 is estimated by inverse distance weighted interpolation with elevation as
5 additional predictor.

1 **Table 2.** Parameters and value ranges for Hydrus-1D modelling.

	Parameter	Value/Range	Unit	Source / calculation method
	Soil hydraulic parameter			
Θ_r	Residual soil water content ^b	0 – 0.3	m ³ /m ³	Calibrated ^a
Θ_s	Saturated soil water content ^b	0.3 – 0.6	m ³ /m ³	Calibrated ^a
α	Van Genuchten parameter related to air entry suction	0.0001 – 0.1	1/mm	Calibrated ^a
n	Van Genuchten parameter related to pore size distribution	1.01 – 3	-	Calibrated ^a
K_s	Saturated hydraulic conductivity	5 – 10000	mm/day	Calibrated ^a
L	Van Genuchten parameter related to tortuosity	-2 – 2	-	Calibrated ^a
	Meteorological parameter			
P	Daily precipitation		mm	Measured time series ^c
T_{max}	Daily maximum temperature		°C	Measured time series ^d
T_{min}	Daily minimum temperature		°C	Measured time series ^d
R_a	Extraterrestrial solar radiation (for Hargreaves equation only)		MJ/m ²	Calculated according to Allen et al. 1998
	Vegetation parameter			
D_r	Rooting depth	0.5 – 1	m	Estimated based on field observations
SCF	Surface Cover Fraction	0.1 – 1	m/m	Estimated based on field observations
LAI	Leaf Area Index		m/m	Calculated according to Šimůnek (2013)
P_0	Fedde's parameter	-100	mm	Hydrus-1D internal database (grass)
P_{0pt}	Fedde's parameter	-250	mm	Hydrus-1D internal database (grass)
P_{2H}	Fedde's parameter	-3000	mm	Hydrus-1D internal database (grass)
P_{2L}	Fedde's parameter	-10000	mm	Hydrus-1D internal database (grass)
P_3	Fedde's parameter	-80000	mm	Hydrus-1D internal database (grass)
r_{2H}	Fedde's parameter	5	mm/day	Hydrus-1D internal database (grass)
r_{2L}	Fedde's parameter	1	mm/day	Hydrus-1D internal database (grass)
α_i	Interception constant	1	mm	Estimated
D_s	Depth of soil profile	0.5 – 1	m	Measured at experimental plots

2 ^a Parameter calibrated for each soil material with SCEM algorithm and Kling-Gupta efficiency as
3 optimization criterion.

4 ^b The upper parameter limit of Θ_r and the lower parameter limit of Θ_s were obtained from the lowest
5 respectively highest measured volumetric soil moisture value of each layer in the respective soil
6 moisture plot.

7 ^c Rainfall at plot SM-2 is estimated by inverse distance weighted interpolation with elevation as
8 additional predictor.

9 ^d Maximum and minimum daily air temperature at the soil moisture plots is estimated by calculation of
10 an elevation-temperature gradient based on meteorological stations in the Jordan Valley and the
11 mountains.

1 **Table 3.** SCEM optimized hydraulic parameter sets for the different plots and probe depths.

Plot	Layer	Θ_r (m ³ /m ³)	Θ_s (m ³ /m ³)	α (1/mm)	n (-)	K_s (mm/day)	L (-)	KGE (-)
SM-1	1 (-10 cm)	0.01	0.41	0.004	1.23	427	2.0	0.91
	2 (-25 cm)	0.12	0.49	0.026	1.30	8159	-2.0	0.94
	3 (-40 cm)	0.11	0.59	0.018	1.54	9468	-2.0	0.90
	4 (-80 cm)	0.10	0.59	0.028	1.36	8732	0.1	0.82
SM-2	1 (-5 cm)	0.00	0.49	0.041	1.18	126	-2.0	0.89
	2 (-10 cm)	0.05	0.40	0.002	1.23	5094	0.6	0.90
	3 (-18 cm)	0.12	0.59	0.012	1.37	9288	2.0	0.87
	4 (-55 cm)	0.13	0.51	0.013	1.43	2679	1.0	0.90
SM-3	1 (-5 cm)	0.00	0.60	0.008	1.23	482	-2.0	0.91
	2 (-10 cm)	0.00	0.56	0.004	1.23	9908	-1.2	0.92
	3 (-20 cm)	0.05	0.46	0.003	1.22	9976	1.2	0.91
	4 (-35 cm)	0.11	0.60	0.001	1.66	5751	2.0	0.94

2

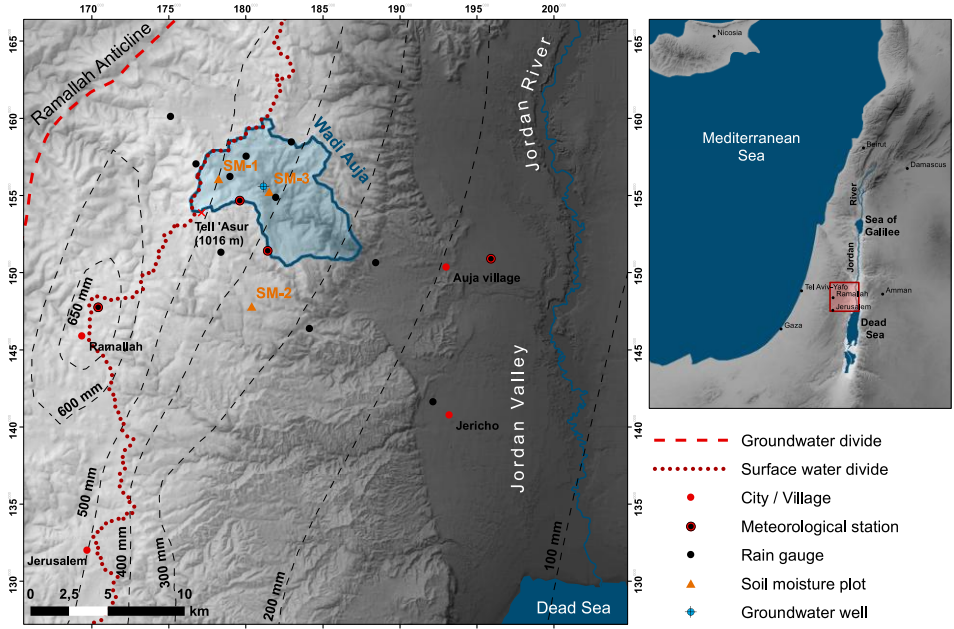
1 **Table 4.** Cumulative sums of the simulated water balance components in mm and % for the
 2 three consecutive hydrological years 2010-2013.

Plot	Year	Rainfall	Interception		Evaporation		Transpiration		Bottom flux	
		(mm)	(mm)	(%)	(mm)	(%)	(mm)	(%)	(mm)	(%)
SM-1	2010/2011	381	62	16	99	26	209	55	13	3
	2011/2012	650	59	9	93	14	209	32	294	45
	2012/2013 ^a	547	39	7	102	19	179	33	224	41
SM-2	2010/2011	248	53	21	81	33	117	47	0	0
	2011/2012	418	55	13	89	21	159	48	118	28
	2012/2013 ^a	346	33	10	84	24	127	37	101	29
SM-3	2010/2011	237	47	20	119	50	84	35	2	1
	2011/2012	436	53	12	120	27	130	30	135	31
	2012/2013 ^a	380	30	8	111	29	105	28	125	33

3 ^a The hydrological year 2012/2013 was modelled until 30th of April 2013.

4

1 **Figures**



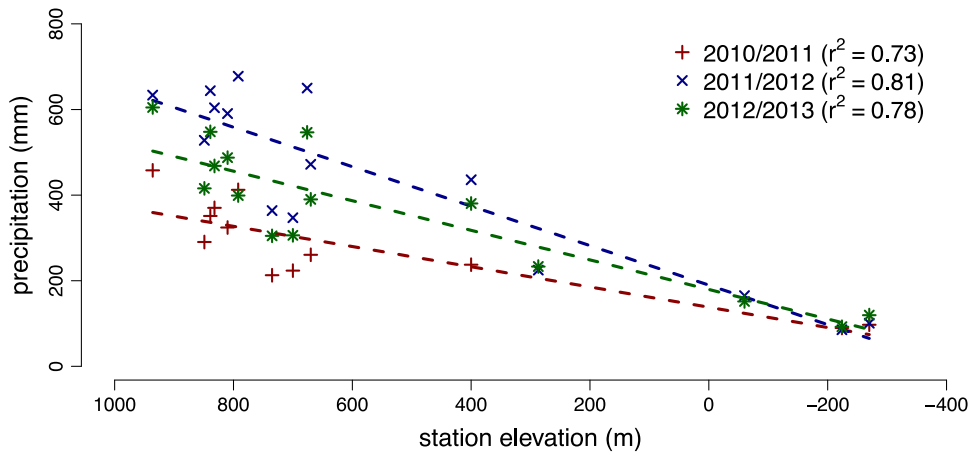
3 **Figure 1.** Study area with location of meteorological stations, rain gauges, soil moisture plots
4 (SM-1, SM-2, SM-3) and isohyets of long-term average annual rainfall (≥ 20 years)
5 according to data from ANTEA (1998). Coordinates in the detailed map are in Palestinian Grid format.

6 Add the location of the Auja Spring

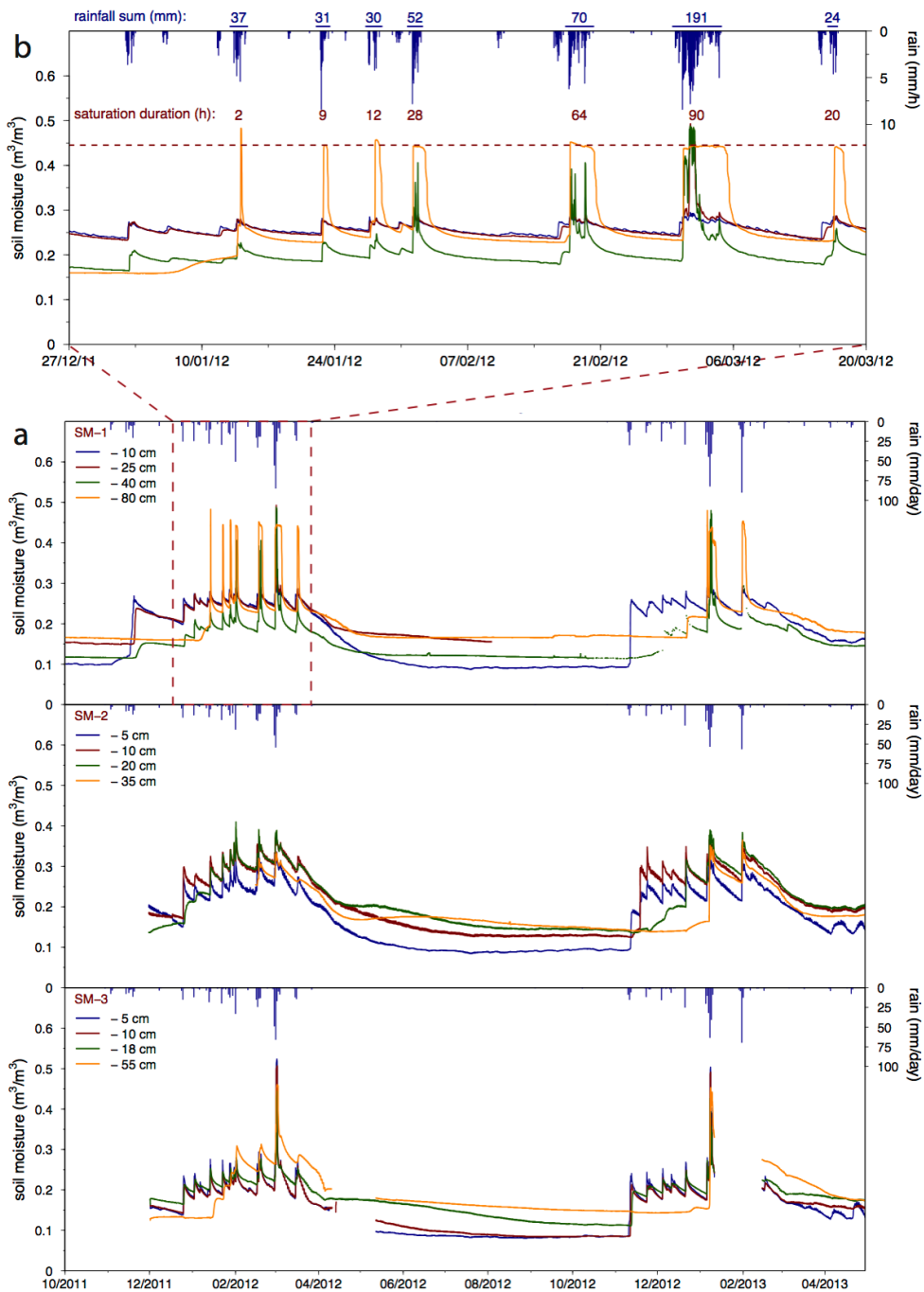
Formatted: Highlight



1
2 **Figure 2.** Typical hillslopes in the study area. The image shows the plain of Ein Samia with
3 semi-arid climatic conditions, where the valley bottom is used for partly irrigated agriculture
4 and the hillslopes are used as extensive grazing land for goats and sheep.

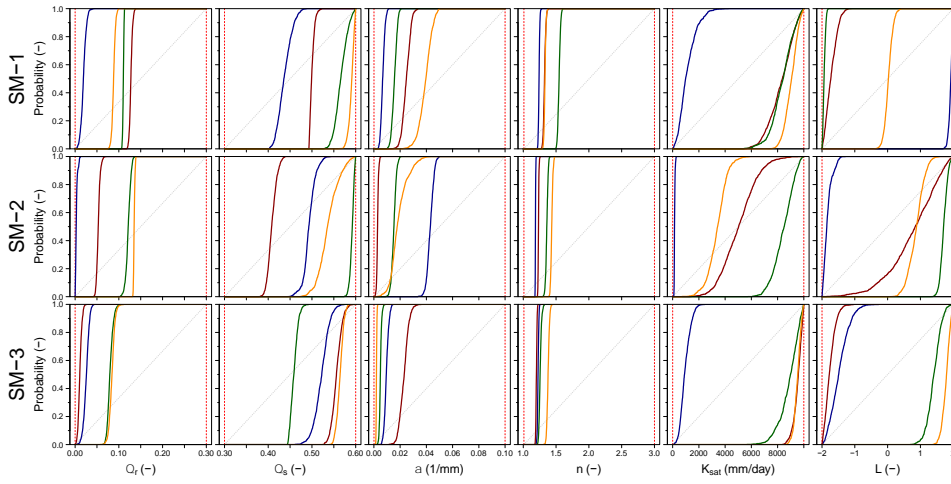


1
 2 **Figure 3.** Correlation between average annual rainfall and station elevation for the individual
 3 hydrological years during the observation period 2010-2013.



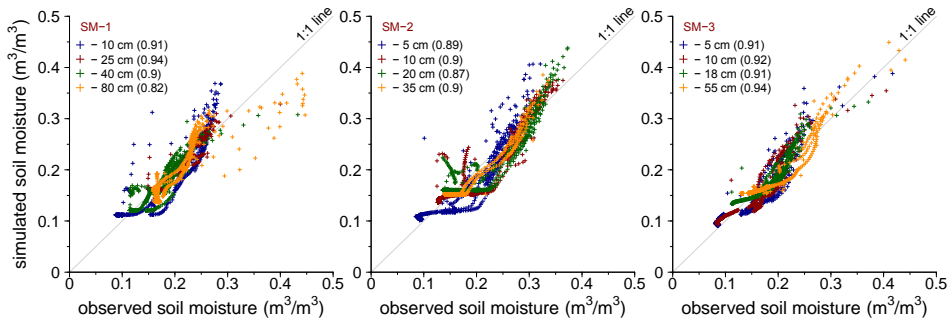
1
2 **Figure 4.** Observed volumetric soil moisture at different depths of the three experimental
3 plots during the complete monitoring period (**ab**) and details on the winter season 2011/2012
4 for plot SM-1 (**ba**).

1

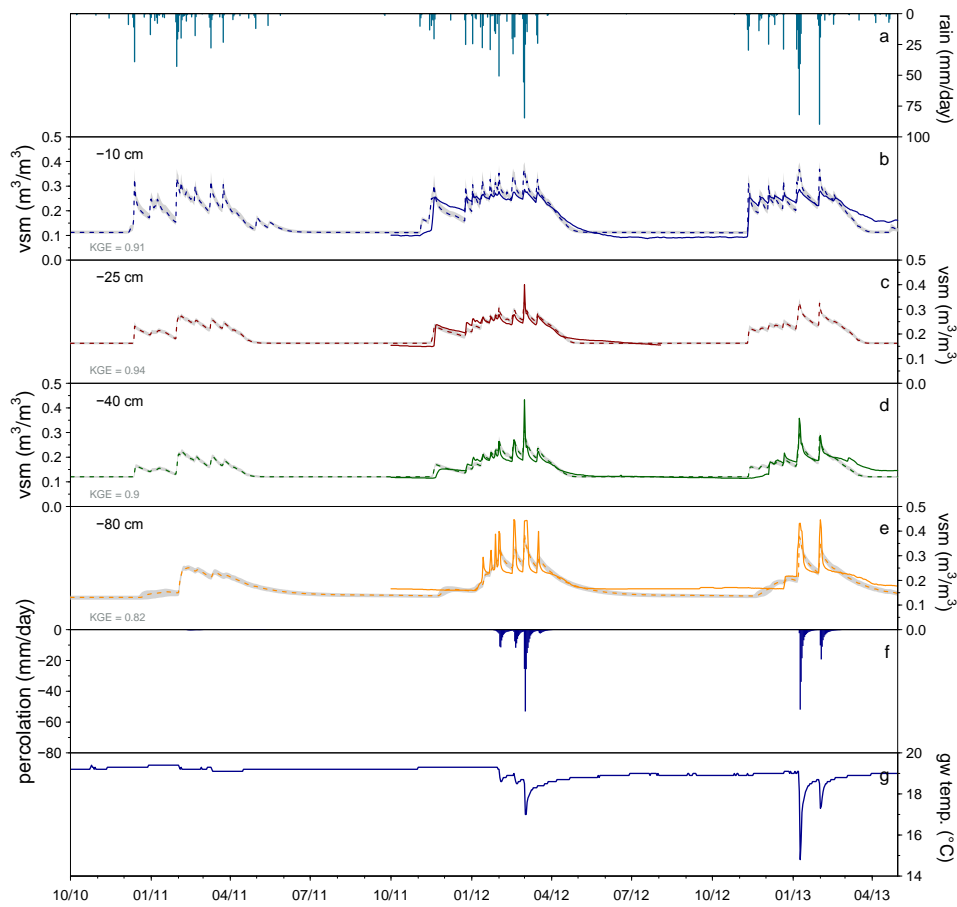


2

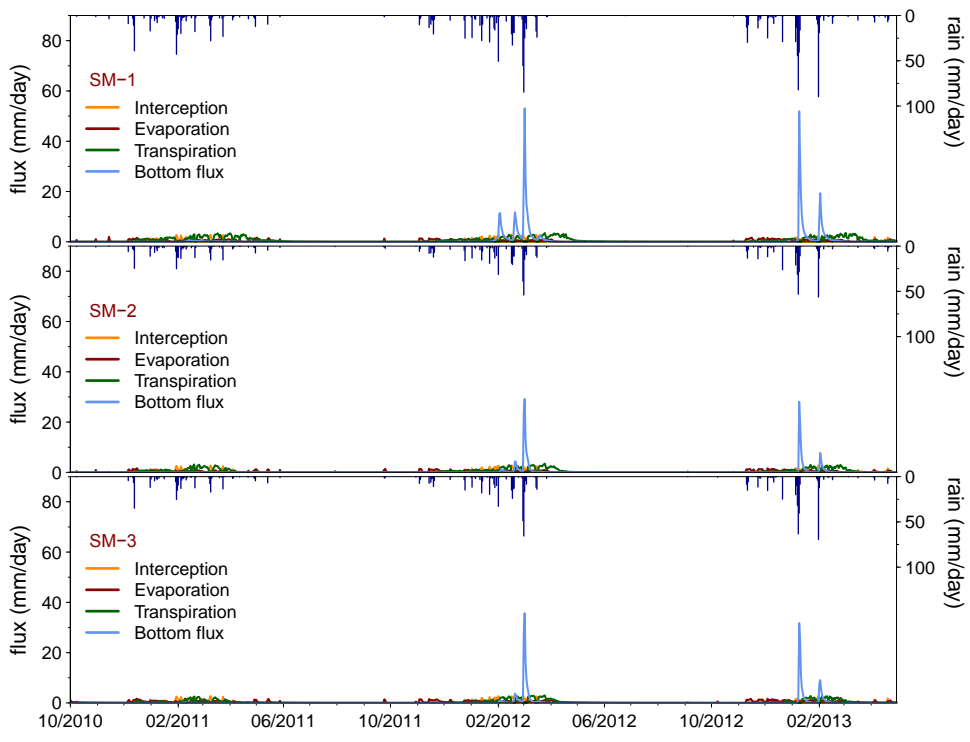
3 **Figure 5.** Cumulative distribution functions of parameters following 1000 model runs after
4 convergence. The line colours correspond to the various soil depths (see Figure 6). The limits
5 of the x-axis represent the selected parameter ranges.



1
 2 **Figure 6.** Measured against simulated volumetric soil water content for the three soil moisture
 3 plots (SM-1, SM-2, SM-3) at individual depths for the simulation period. KGE values are
 4 shown in brackets in the legend.

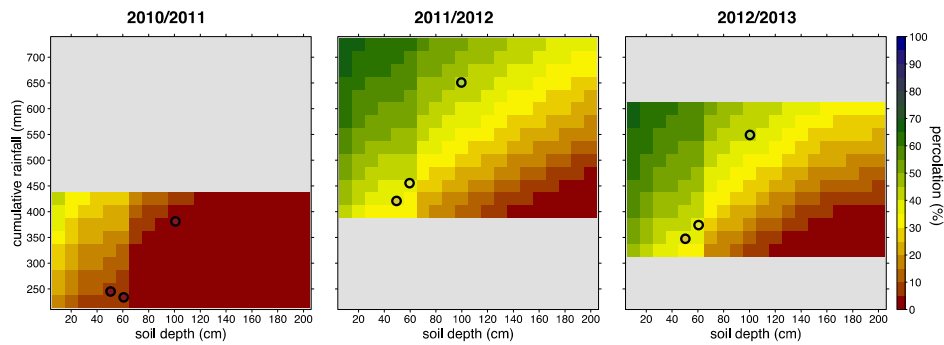


1
2 **Figure 7.** Time series of rainfall (a), simulated and observed volumetric water content for soil
3 moisture plot SM-1 (b-e), Hydrus-1D simulated percolation (f) and water temperature in a
4 nearby groundwater well (g). The grey shaded area represents the 95 % confidence interval of
5 soil moisture based on model parameter sets obtained using SCEM after fulfilment of the
6 convergence criterion.



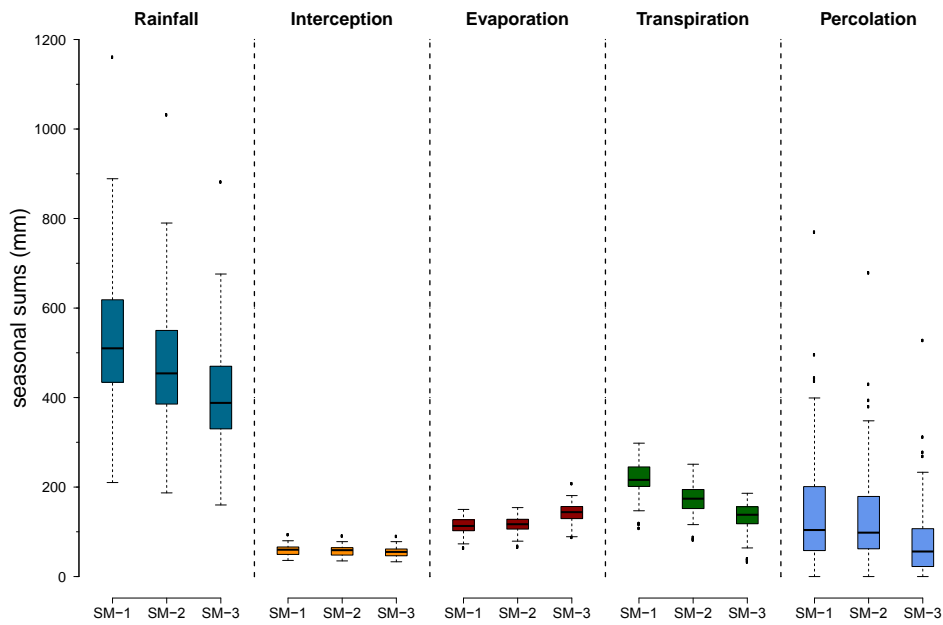
1
 2 **Figure 8.** Simulated daily water fluxes at the single soil moisture plots for the simulation
 3 period 2010-2013. **The interception, evaporation and transpiration can hardly be seen. Also,**
 4 **are they really so low?**

Formatted: Highlight

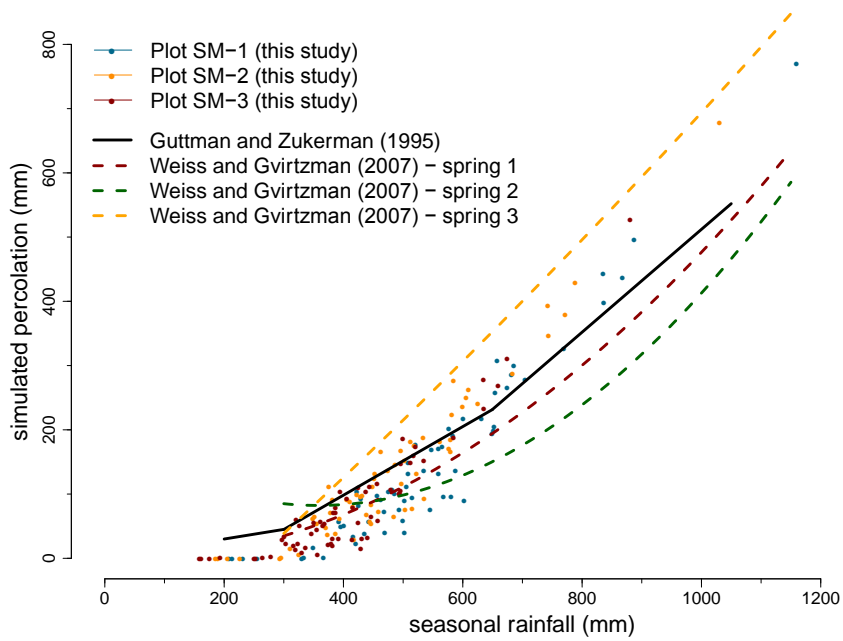


1

2 **Figure 9.** Simulated percolation versus soil depth and rainfall amounts along the climatic
3 gradient for three consecutive winter seasons with different rainfall depths and distribution
4 patterns. Simulations were based on calibrated soil hydraulic properties of plots SM-1. The
5 grey shaded areas display rainfall depths, which have not been reached in the study area
6 within altitudes of 400 to 1000 m a.s.l. according to calculated rainfall gradients. The points
7 represent the plot scale simulated percolation fluxes using optimal parameter sets for the
8 single plots SM-1, SM-2 and SM-3.



1
2 **Figure 10.** Seasonal sums of simulated water balance components for the period 1951 to 2013
3 using the calibrated soil hydraulic parameters of the various plots. Rainfall and temperature
4 data were obtained from the nearby Jerusalem central station (<http://www.data.gov.il/ims>) and
5 corrected for the single locations by applying a simple elevation gradient-based correction
6 factor.



1

2 **Figure 11.** Simulated seasonal percolation at the plot scale (SM-1, SM-2, SM-3) for the
 3 period 1951-2013 in comparison ~~to with~~ rainfall-recharge relationships for the carbonate
 4 aquifer (Guttman and Zukerman, 1995) and three small karst springs emerging from local
 5 perched aquifers (Weiss and Gvirtzman, 2007).